Contents lists available at ScienceDirect

Journal of Saudi Chemical Society

journal homepage: www.ksu.edu.sa

# Transforming volcanic mud into mesoporous silica xerogel and its performance for efficient humidity adsorption

Qurrota A'yuni [a,b,*], Ardhana Rahmayanti [c], Hartati Hartati [a,*], Purkan Purkan [a], Riki Subagyo [d], Sofia Fuadah [a], Novia Amalia Sholeha [e], Hasliza Bahruji [f], Hikmat Hikmat [g]

[a] Department of Chemistry, Faculty of Science and Technology, Universitas Airlangga, Campus C UNAIR, Mulyorejo 60115, Surabaya, Indonesia
[b] Department of Chemical Engineering, Faculty of Engineering, Universitas Nahdlatul Ulama Sidoarjo, Jl. Lingkar Timur KM 5,5 Rangkah Kidul, Sidoarjo 61234, Indonesia
[c] Department of Environmental Engineering, Faculty of Engineering, Universitas Nahdlatul Ulama Sidoarjo, Jl. Lingkar Timur KM 5,5 Rangkah Kidul, Sidoarjo 61234, Indonesia
[d] Department of Chemistry, Faculty of Science and Data Analytics, Institut Teknologi Sepuluh Nopember, Kampus ITS Keputih, Sukolilo 60111, Surabaya, Indonesia
[e] College of Vocational Studies, Bogor Agricultural University (IPB University), Jl. Kumbang No. 14, Bogor 16151, Indonesia
[f] Centre for Advanced Material and Energy Sciences, Universiti Brunei Darussalam, Jl. Tungku Link, Gadong BE1410, Brunei Darussalam
[g] Research Center for Chemistry, National Research and Innovation Agency of Indonesia (BRIN), Gd. 452 Bldg, PUSPIPTEK Area, Tangerang Selatan, Banten 15314, Indonesia

ARTICLE INFO

*Keywords:*
Silica xerogel
Volcanic mud
Hazardous waste
Humidity adsorption
pH effect

ABSTRACT

A high humidity level in the environment leads to the development of desiccants as hygroscopic material for adsorbing water vapor. Mesoporous silica xerogel, one of the solid adsorbents used for humidity adsorption, was synthesized from hazardous waste of volcanic mud via sol–gel methods by controlling the pH of the solution. The disordered amorphous silica was obtained, with the properties varied depending on the pH of the solution. Silica xerogel obtained at pH 8 exhibits the highest specific surface area of 576.527 $m^2g^{-1}$ and mesoporous surface area of 527.842 $m^2g^{-1}$. It also has the highest adsorption capacity of 18.90% $g_w/g_{ads}$ determined from the conventional method and 22.14% $g_w/g_{ads}$ from TG analysis. The performance for humidity adsorption exceeds the commercial silica with an efficiency of 0.9–7% $g_w/g_{ads}$. This result indicates that the potential $SiO_2$ extracted from volcanic mud can be commercialized as desiccants for humidity adsorption.

## 1. Introduction

Water vapor is a crucial indicator affecting agricultural and industrial production, indoor comfort, and environmental quality [1,2], as its presence can alter the material and ecological stability. Accordingly, it is essential to control humidity at room temperature using proper dehumidification techniques. Several methods for dehumidification are developed, including refrigeration dehumidification [3], aeration dehumidification [4], liquid absorption dehumidification [5,6], and solid adsorption dehumidification [7,8]. Dehumidification via adsorption allows moisture adsorption in an ambient condition through surface functional groups of solid adsorbent (i.e., hydroxyl group) and textural properties (e.g., surface area, pore size, and diameter). Solid adsorption dehumidification techniques offer several advantages, such as low dew point temperature, large adsorption area, providing good regeneration efficiency, and environmental friendliness [9]. Solid adsorption dehumidification techniques also have an excellent prospect in various applications, such as industrial processes, preservation and storage, maintaining indoor air quality, desiccant cooling systems, and energy efficiency [10–12].

Solid adsorbents for dehumidification are continuously being developed to improve their performance by considering several parameters, such as adsorption capacity, chemical stability, selectivity, regeneration ability, affordable cost, and availability. Silica xerogel (SX) has been developed for commercial use of solid desiccant materials [13,14]. The pore structure and surface silanol group allow rapid humidity adsorption [15,16]. The pore and surface area of silica can be altered by various synthesis parameters to improve water adsorption [17,18]. Apart from that, SX can be synthesized from various natural sources, which is very advantageous to enhance the economic value of

* Corresponding authors.
*E-mail addresses:* qurrota.ayuni@fst.unair.ac.id (Q. A'yuni), hartati@fst.unair.ac.id (H. Hartati).

https://doi.org/10.1016/j.jscs.2023.101771
Received 26 July 2023; Received in revised form 12 November 2023; Accepted 19 November 2023
Available online 21 November 2023
1319-6103/© 2023 The Author(s). Published by Elsevier B.V. on behalf of King Saud University. This is an open access article under the CC BY-NC-ND license (http://creativecommons.org/licenses/by-nc-nd/4.0/).

natural sources. Using natural sources is an alternative way to replace the expensively commercial silicon alkoxides precursors [19–21]. Volcanic mud (VM) from the 2006 eruption in Sidoarjo district, which has polluted the surrounding environment and is considered hazardous waste, contains a high silica content that can be converted to silica xerogel [22,23].

The Sol-gel method is a known method for the synthesis of silica xerogel with various geometry structures and particle sizes [24,25]. The polycondensation process must be controlled to create large pores, surface area, and textural properties of silica xerogel [26]. The pH of the solution influences the Si–O–Si polymerization process, which according to Bust et al. that reported the highest polymerization rate occurs at pH 7 and 8 [27]. When in acidic and alkaline pH, the polymerization rate of silica will be lower. The purity of silica obtained also be low when a gelation pH < 7 was used [28]. Besides that, pH also affects the number of hydroxyl groups on the surface, which is very important for water molecule adsorption.

In this study, volcanic mud (VM) was used as a precursor for SX synthesis. VM was utilized as precursor of SX synthesis due to the high silica content in VM (approximately 53.40%) and various metal oxide content, which has been used for adsorption [23], transesterification process, and biofuel production [29]. Silica was extracted via acid leaching methods followed by heat treatment. The obtained silica-rich VM was used to prepare silica xerogel via sol–gel method with ambient pressure drying. The pH on gelation was varied from pH 6 to pH 10 to form silica with different textural properties that can influence humidity adsorption. The humidity adsorption was carried out using conventional method and thermal gravimetric (TG) analysis. The synthesised silica was compared with the commercial silica gel to observe the potency and effectiveness of the product. Finally, the correlation between the textural properties of silica and the humidity adsorption was discussed to understand the effect of pH variation during sol–gel synthesis.

## 2. Methodology

### 2.1. Materials

VM was obtained from Sidoarjo district, East Java, Indonesia, commonly called Lapindo mud. Hydrochloric acid (HCl, 37%) and Sodium hydroxide (NaOH, 99%) were purchased from Merck Millipore. Demineralised water was used to dilute HCl and NaOH, and in washing process.

### 2.2. Preparation of VM

VM was dried at 100 °C for 24 hours to remove the water content. The dried VM was crushed and sieved into 140 mesh to obtain the uniform particle size. 200 grams of VM powder was mixed with 1000 mL of HCl 5 M. The mixtures were stirred at 60 °C for two hours. Then, the mixture was left until the two phases (powder and filtrate) were formed. The yellowish filtrate was then separated via decantation process. The obtained powder was washed by adding water until the pH is close to neutral. The mixtures were left for a night followed by decantation process to remove the filtrate. This process was conducted several times until the filtrate of the mixtures was changed into transparent. The obtained powder was dried at 100 °C for 24 hours and noted as VML. The dried powder was annealed at 680 °C for one hour under atmospheric conditions. The obtained powder was labelled as VMLT.

### 2.3. Synthesis of SX

The synthesis of SX was carried out by sol–gel method. In order to obtain sodium silicate ($Na_2SiO_3$), 10 grams of VMLT powder was added into 100 mL of NaOH solution (2 M). The mixture was reacted at 90 °C for one hour using simple reflux process. The mixtures were cooled naturally and filtered to obtain $Na_2SiO_3$ solution.

SX was fabricated by adding HCl (1 M) and/or NaOH (0.5 M) via titration process to achieve various pH such as 6, 7, 8, 9, and 10. Due to the pH of $Na_2SiO_3$ solution was 13, the silica xerogel with pH of 9 and 10 was carried out by adding HCl. Due to the SX was formed at pH of 9, the preparation of SX with pH of 6, 7, and 8 was done by the addition of HCl until the pH solution of 4 was reached. Then, the solution with pH of 4 was added with NaOH solution to generate the silica xerogel with pH of 6, 7, and 8. The amount of HCl and/or NaOH was summarized in Table 1. The obtained xerogel was aged and washed to remove the formed salt on gel. The xerogel was dried at 80 °C for 18 hours. The resulted powder was labelled as SX*n* (*n* = pH).

### 2.4. Characterization

The composition of volcanic mud, volcanic mud after leaching process, and volcanic mud after leaching and heating treatment was analysed using X-ray fluorescence (XRF) spectroscopy. The structural property of Lapindo mud, Lapindo mud after leaching process, Lapindo mud after leaching and heating treatment, and silica xerogel was characterized using X-ray diffraction (XRD) technique. The functional group in the synthesized silica xerogel was determined using Fourier transform infrared (FTIR) spectroscopy. Scanning electron microscopy (SEM) was utilized to investigate the morphology of the prepared silica xerogel followed by Energy dispersive X-ray (EDX) analysis to determine the element composition in the prepared silica xerogel. The textural properties of the obtained silica xerogel were investigated using $N_2$ adsorption–desorption technique. The detailed analysis conditions are summarized in Table 2.

### 2.5. Humidity adsorption

Silica xerogel was heated at 120 °C for one hour to remove the water content on the silica xerogel. The dried silica xerogel was weighed before the adsorption process. The dried silica xerogel was placed into a desiccator, which placed a glass of water inside it. The relative humidity (RH) in desiccator was regulated to be 70%, 80%, and 90% at the ambient temperature of 29 ± 1 °C. This process was carried out for 180 minutes. The change of mass was recorded every 30 minutes. The adsorption capacity was calculated using Eq. (1).

$$Adsorption\ capacity = \frac{mass\ of\ water\ on\ silica\ xerogel}{mass\ of\ silica\ xerogel} \times 100\% \quad (1)$$

In order to compare their performance, the commercial silica gel was also used for humidity adsorption at similar conditions. Five types of commercial silica gel were used in the humidity adsorption studies at RH of 70%.

The thermal gravimetric analysis (TGA) was conducted to verify the performance which was investigated via conventional methods. The prepared silica xerogel was dried and placed into the desiccator with controlled RH. Then, the silica xerogel was analysis using TGA to obtain weight loss profile. The detailed analysis process can be seen in Table 2. The adsorption capacity was calculated at 100 °C following the Eq. (2)

**Table 1**
The amount of HCl and/or NaOH in the preparation of silica xerogel.

| pH of solution | pH of $Na_2SiO_3$ | Volume (mL) | | Labelling |
|---|---|---|---|---|
| | | HCl (1 M) | NaOH (0.5 M) | |
| 6 | 13 | 200 | 1 | SX6 |
| 7 | 13 | 236 | 2.9 | SX7 |
| 8 | 13 | 200 | 6.5 | SX8 |
| 9 | 13 | 225 | - | SX9 |
| 10 | 13 | 177.3 | - | SX10 |

**Table 2**
The detail analysis conditions of samples.

| Technique of samples characterization | Instruments | Conditions |
|---|---|---|
| XRF | PANalytical, MiniPal 4 energy-dispersive XRF Bench-Top spectrometer | Samples were washed using acetone and placed into the sample holder. Then, the samples were measured seven times to form the calibration for each element. After that, the samples were measured and recorded at 16 kV and 100 μA for 5 minutes. |
| XRD | PANanlytical X'Pert MPD No. 1 | Using Cu Kα (λ = 1.5405 Å) in the 2θ range of 5–90°, operated at 30 mA and 40 kV. The scanning rate was 0.017°/second |
| FTIR | Shimadzu IR Tracer-100 | 5 mg of silica xerogel was mixed with 100 mg of KBr (1:20) and the powders was measured and recorded at wavenumber of 4000–400 $cm^{-1}$ |
| FESEM-EDX | Jeol JIB-4610F Multi Beam System | We used gold coating on silica xerogel for FESEM analysis, equipped with EDX analysis. The samples was vacuumed using 20 mA for two minutes and analysed at an accelerating voltage of 15 kV, 500–20.000 magnification, and 1.0 μm micron marker. |
| $N_2$ adsorption–desorption | Quantachrome Quadrasorb - Evo Surface Area & Pore Size Analyzer | The samples were degassed at 300 °C under vacuum followed by flowing $N_2$ gas over the samples at 77 K. The surface area of samples was measured using Brunauer–Emmett–Teller (BET) methods, whereas the pore size distribution was analysed using Non-Local Density Functional Theory NLDFT methods. |
| TGA/DTA | Mettler Toledo | Operated at 27–600 °C under nitrogen flow with the heating and flowing rate of 5 °C $min^{-1}$ and 30 mL $min^{-1}$, respectively. |

$$Adsorption\ capacity = \frac{mass\ of\ silica\ xerogel\ at\ 100°C}{initial\ mass\ of\ silica\ xerogel} \times 100\% \quad (2)$$

## 3. Results and discussion

### 3.1. Characterization

XRF analysis was used to analyse the composition of the VM, VML, and VMLT in the form of oxide compound, as summarized in Table 3. According to the result, volcanic mud is composed of $SiO_2$, $Fe_2O_3$, $Al_2O_3$, CaO, and several metal oxides, similar to the previous results reported by Jalil et al. [23] and Rahmayanti et al. [30]. $SiO_2$ is the major constituent of VM, which is very suitable to utilize as the SX precursor. The acid leaching process was carried out to dissolve the metal oxide composition in VM. After the acid leaching process, the $SiO_2$ content is increased due to the removal of metal oxide impurities in VM. According to Table 3, $Fe_2O_3$ and CaO composition is reduced after the acid leaching process, indicating a high solubility of $Fe_2O_3$ and CaO in HCl. The thermal process also enhanced the $SiO_2$ content and reduced the $Fe_2O_3$ content, demonstrating that the combination of acid leaching and thermal treatment efficiently increases the $SiO_2$ content in the VM [31,32]. However, the composition of $Al_2O_3$ does not change after the acid leaching and thermal treatment, showing that 5 M HCl is not strong enough to dissolve $Al_2O_3$ in volcanic mud [33]. Moreover, these pretreatments enhance the mud's reactivity for easy extraction by alkalis.

The diffraction pattern of VM, VML, VMLT, and the prepared silica xerogel (SX8 as the optimum silica xerogel) is depicted in Fig. 1. VM consists of several minerals including quartz ($SiO_2$), lipscombite ($Fe_{1.473}HO_5P$, ICSD No. 96–900–1208), bavenite ($Al_2Be_2Ca_4H_2O_{28}Si_9$, ICSD No. 96–900–7488) and chloritoid ($Al_{3.983}Fe_{1.038}H_4Mg_{0.97}O_{14}Si_2$, ICSD No. 96–900–5443). The sharp characteristic peak of quartz at 2θ = 26.55° (ICSD No. 96–900–5019) indicates the presence of high crystalline quartz in VM. The intensity of the quartz peak is enhanced in VML after the acid leaching process, indicating quartz is stable in HCl. The quartz peak is more intensively pronounced in VMLT after heat treatment. The results suggest most of the minerals were removed while the quartz was unaffected during acid leaching and heat treatment, so these processes can concentrate the quartz content in VM, which agrees with XRF results. After the sol–gel process, the obtained silica xerogel exhibits a broad peak of $SiO_2$ at wide-angel between 22° and 30°, showing the generation of amorphous $SiO_2$ as skeleton particles. This result is similar to previous work by Steven et al. that synthesized amorphous silica gel from rice husk ash [34].

**Table 3**
The composition of volcanic mud after acid leaching and thermal treatment.

| Compound | Particle composition | | |
|---|---|---|---|
| | VM | VML | VMLT |
| $SiO_2$ | 48.32 | 68.13 | 68.52 |
| $Fe_2O_3$ | 28.78 | 14.19 | 13.58 |
| $Al_2O_3$ | 13.96 | 14.14 | 14.26 |
| CaO | 7.69 | 3.00 | 3.14 |
| SrO | 0.39 | 0.10 | 0.08 |
| MnO | 0.45 | 0.09 | 0.08 |
| CuO | 0.15 | 0.12 | 0.12 |
| $ZrO_2$ | 0.12 | 0.11 | 0.10 |
| $V_2O_5$ | 0.09 | 0.08 | 0.08 |
| $Rb_2O$ | 0.05 | 0.04 | 0.04 |

FTIR spectra of VM and the prepared silica xerogel are depicted in Fig. 2. All samples show a broad absorption peak at 3400–3000 $cm^{-1}$, indicating the stretching vibration of silanol group (Si—OH) [35]. The absorption band at 1650–1600 $cm^{-1}$ is attributed to the bending vibration of —OH group in Si—OH [32,36]. The asymmetry stretching vibration of Si—O in Si—O—Si is observed at 1200–1000 $cm^{-1}$, whereas the symmetry stretching vibration of Si—O in Si—O—Si is shown at 980–800 $cm^{-1}$ [37,38]. The absorption band at 950 $cm^{-1}$ is associated with the symmetry stretching vibration of Si—O in Si—OH [39]. The growth of the Si—OH peak at 950 $cm^{-1}$ reduces the intensity of the Si—O—Si peak at 1200–1000 $cm^{-1}$, thus increasing the hydrophilic characteristics of silica xerogel [40]. The formation of interrelated siloxane and silanol groups is influenced by pH control. SX8 has the highest absorption intensity at 950 $cm^{-1}$, which indicates SX8 has more hydrophilic properties than the other SX. Especially for VM spectra, the absorption band at 1500–1300 $cm^{-1}$ indicates the presence of hydrocarbon compound (C—H vibration) on VM because no leaching or heat treatment was conducted in the pre-preparation. The hydrocarbon compound on VM originates from liquefied petroleum and natural gas, which consist of methane, ethane, propane, and butane. The absence of absorption bands at 1500–1300 $cm^{-1}$ in the prepared silica xerogel reveals that the hydrocarbon compound on VM has been decomposed after leaching and heat treatment.

The textural properties of VM and the prepared silica gel are analysed by $N_2$ adsorption–desorption technique as shown in Fig. 3. VM has a low specific surface area (17 $m^2g^{-1}$) and low pore volume (0.06 $cm^3g^{-1}$). Each SX exhibits a different nitrogen adsorption profile. The nitrogen uptake of SX6 is slightly enhanced, followed by the formation of small hysteresis loops at $P/P_0$ = 0.4–0.8 due to the capillary condensation. SX7 generated a significant enhancement of nitrogen uptake at the initial stage of adsorption until the end of adsorption. SX7 also exhibited a high nitrogen uptake compared to others. Similarly, the significant enhancement of nitrogen uptake was also yielded by SX8. SX9 and SX10 exhibit a similar feature of nitrogen uptake. At the initial stage of adsorption ($P/P_0$ 0.1–0.65), the amount of adsorbed nitrogen is

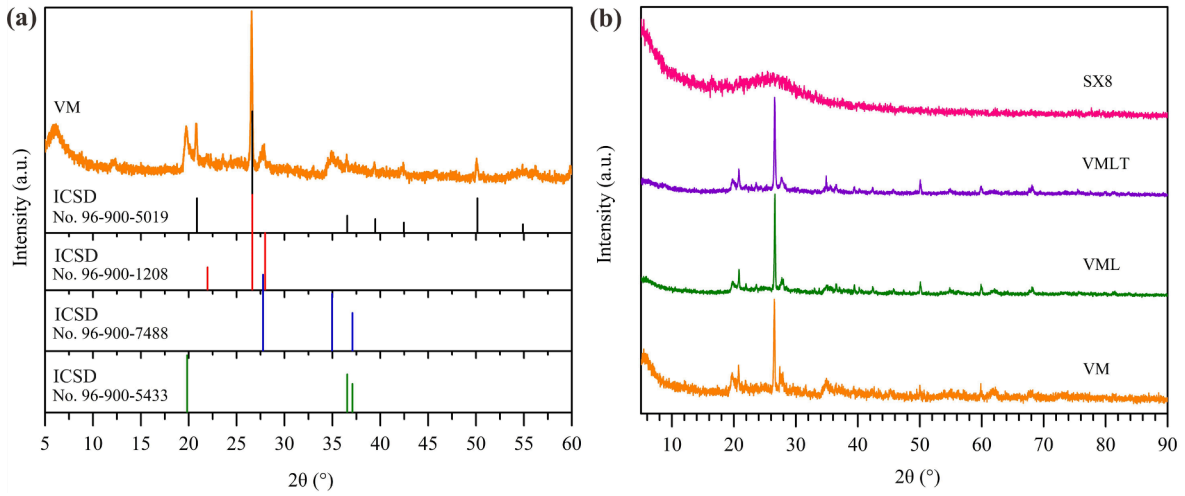


**Fig. 1.** (a) Diffractogram of VM with the ICSD data. (b) Comparison of diffractograms of samples before and after acid leaching-heat treatment followed by sol–gel process.

slightly increased, followed by a significant increase in nitrogen adsorption. According to the IUPAC classification, all samples are categorized to the type IV isotherm, revealing that all samples are mesoporous materials [41,42]. As summarized in Table 4, SX8 exhibits the highest specific surface area and mesopore surface compared to others, indicating that SX8 has a high number of sites for the adsorption process. However, increasing pH to 9 and 10 reduced the surface area.

Interestingly, the difference in pH adjustment during the sol–gel synthesis generates two types of hysteresis loop. Adjusting pH to 6, 7, and 8 resulted in the Silica with H2 type hysteresis loop, commonly observed when a network of interconnected ink bottle pores with a small mesopore diameter is present, which may be formed by the particle aggregation. SX9 and SX10 generate H1 type hysteresis loops, attributing them to the cylindrical or tubular type of pores with a narrow distribution of uniform particles. The results are depicted in Fig. 3b. SX9 and SX10 showed the highest pore diameter at 11.680 nm and 10.488 nm, respectively. Furthermore, the gelation pH was found to affect the surface area and the pore size of silica xerogel.

Interestingly, the yielded surface area of SX is varying. According to the process, the formation of SX9 and SX10 was carried out by adding HCl, which has a slight effect on pore formation. Consequently, the resulting surface area of SX9 and SX10 is low. The formation of SX6–SX8 was conducted by adding HCl until the pH solution of 4 was reached. Adding NaOH to achieve the pH solution of 6–8 is beneficial for controlling the formation of pores in hydrogel and improving the surface area. However, the surface area of SX7 is slightly decreased compared to the surface area of SX6. It might be correlated with the formation of particle aggregation during the crystallization process, which affected the surface area of samples.

To understand the findings mentioned earlier, we need to consider the theory of silica polymerization. This process is affected by various factors, but the most important ones are gelation pH and electrostatic interaction [43]. In the first instance, VMLT is treated with sodium hydroxide solution then silica from volcanic mud dissolves by forming $Na_2SiO_3$ according to the following chemical reaction (Eq. (3)):

$$SiO_{2(\text{volcanic mud})} + 2NaOH_{(aq)} \rightarrow Na_2SiO_{3(aq)} + H_2O_{(l)} \quad (3)$$

Furthermore, acidification and condensation occur simultaneously during silica xerogel production. The acidification process is a hydrolysis reaction of sodium silicate to produce orthosilicic acid which will become silica xerogel (Eq. (4)). It can be expressed as follows:

$$Na_2SiO_{3(aq)} + 2HCl_{(aq)} \rightarrow SiO_{2(s)}\downarrow + 2NaCl_{(aq)} + H_2O_{(l)} \quad (4)$$

Moreover, the condensation process begins with a reaction between the silanol group ≡Si—OH with another ≡Si—OH from the hydrolysis reaction to create a siloxane linkage [44]. It can be expressed as:

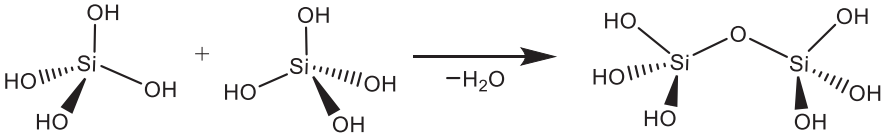


(5)

The initial pH of the sodium silicate solution is 13, and then hydrochloric acid is added for the acidification process as Eq. (4). Silica precipitation starts when the pH decreases to less than 11. At pH < 9, obtaining the desired pH is difficult because adding a small quantity of acid causes a drastic change in pH to 4. The sodium silicate solution immediately forms a hydrogel at a pH around neutral (pH 6, 7, 8). Therefore, the addition of sodium hydroxide is required, as in Table 1. These results show that the aggregation rate will accelerate with a decrease in gelation pH due to an increase in salt concentration (Eq. (4)). The presence of $Na^+$ ions during the reaction will accelerate the condensation reaction (Eq. (5)). These ions will interact with the negatively charged silicate species and screen the surface charge of the particles which can favor their aggregation followed by coagulation, so makes it possible to form a hydrogel directly. Whereas at high gelation pH, in the absence of salt, electrostatic interactions between negatively charged particles limit the aggregation process to form a three-dimensional network of porous silica gel, so affecting the Oswald ripening process.

FESEM micrographs of VM and SX6–SX10 are presented in Fig. 4 images recorded at different magnifications (left: ×500, middle:

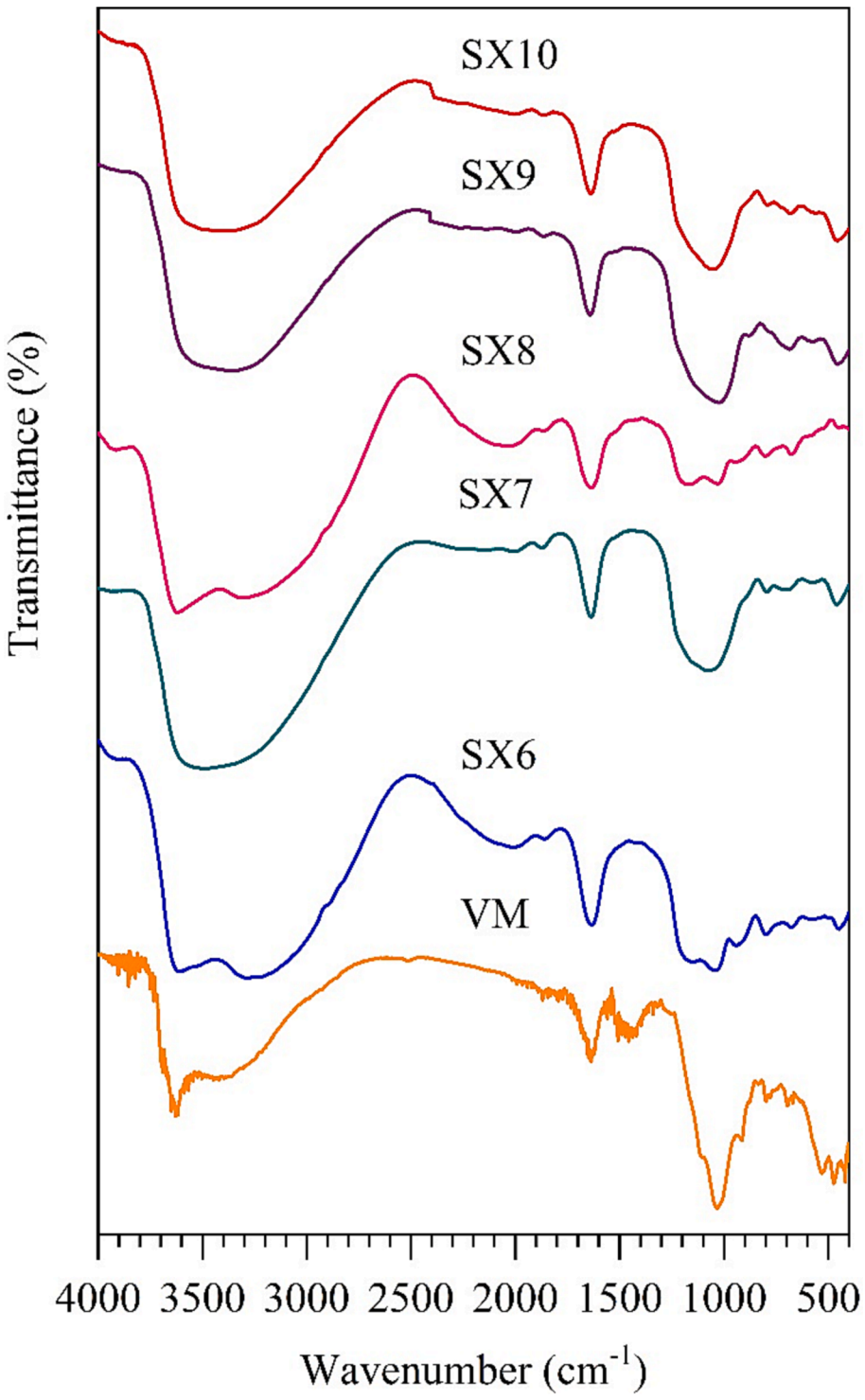


**Fig. 2.** FTIR spectra of VM and SX in difference of pH synthesis.

×3.000, and right: ×20.000). The survey images (Fig. 4, left) show distinct differences in the micromorphology of compacted or agglomerated matter. As the precursor, VM exhibits the sheets-like morphologies (see Fig. 4a, left) connected to each other and form large particle sizes in micrometers. VM morphology is in line with the mineral of hectorite organo-clay, showing compact surfaces [45]. Transforming VM to SX generates different morphology. SX is formed by aggregates strongly agglomerated in a microscopic arrangement and partly shows open intergranular volumes (Fig. 4b-f). In low magnification (see Fig. 4b-f, left), SX6–SX10 show big particles with irregular shape and irregular size, which is in line with a previous study by Prempeh et al. [46] that synthesized silica by using cornhusk as the silica sources. SX6 (Fig. 4b) and SX8 (Fig. 4d) show dense microparticles formed by strong agglomeration and show the presence of grain boundaries. Meanwhile, the spheres-like particles are observed in SX7, SX9, and SX10 (Fig. 4c, e, and f, respectively). The spheres-like particles connected each other to form big particles. Small aggregates are also observed scattered on the surface of big particles, demonstrating the uncompleted crystallization process [38]. The presence of small particles on the surface of big particles was also reported in the previous study by Sriram et al. [47,48]. It

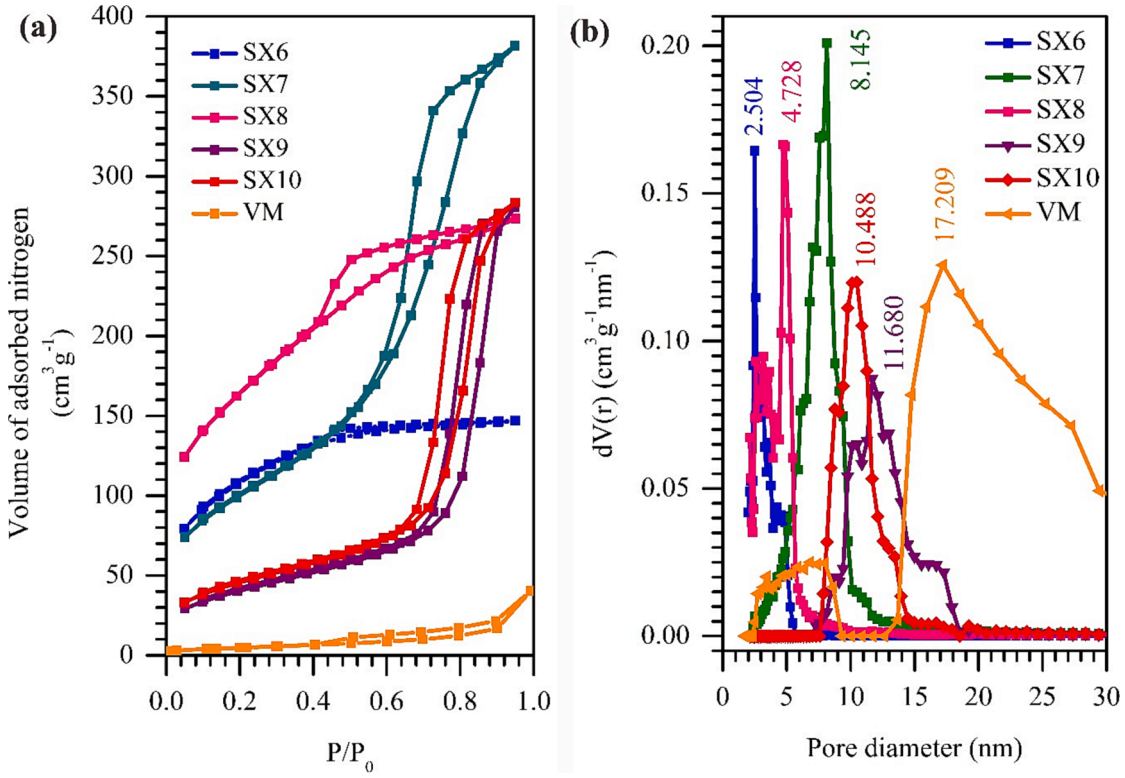


**Fig. 3.** (a) $N_2$ adsorption–desorption and (b) pore size distribution of samples.

**Table 4**
Summary of the textural properties of SX.

| Textural properties | VM | pH | | | | |
|---|---|---|---|---|---|---|
| | | 6 | 7 | 8 | 9 | 10 |
| Specific surface area[a] ($m^2g^{-1}$) | 17.299 | 381.580 | 357.594 | 576.527 | 145.491 | 163.209 |
| Mesopore surface area[b] ($m^2g^{-1}$) | 28.490 | 327.532 | 309.221 | 527.842 | 139.19 | 159.883 |
| Pore volume[b] ($cm^3\ g^{-1}$) | 0.063 | 0.215 | 0.575 | 0.404 | 0.428 | 0.429 |
| Mesopore diameter[b] (nm) | 17.209 | 2.504 | 8.145 | 4.728 | 11.680 | 10.488 |

[a] Measured by BET methods.
[b] measured by NLDFT methods.

has been observed that an increase in pH levels leads to a decrease in particle growth rate [49]. As previously explained, it can be related to the decrease of salt or $Na^+$ ions that can limit the rate of aggregation and condensation. To confirm the element composition of SX, the EDX spectra of SX8 is displayed in Fig. 4g. SX8 consists of Si, O, Na, and Al elements with weight percentage of 38.93, 53.23, 4.52, and 3.33%, respectively. The highest composition of SX8 is O element, which is connected with Si element to generate Si-O configuration in $SiO_2$. Small amounts of Na and Al remain from the precursors that are not lost during wet gel washing or VM pretreatment.

### 3.2. Humidity adsorption

#### 3.2.1. Conventional methods

The humidity adsorption was carried out to observe the effect of textural properties of silica xerogel for the adsorption process. SX has a white fine crystalline appearance and becomes less bright after hydration. As shown in Fig. 5, at RH = 70%, the trend of humidity adsorption at 30 minutes is in line with the trend of the surface area of SX. All samples showed low humidity adsorption at 30 minutes, followed by a slight enhancement of adsorbed water. Especially for SX6, the humidity adsorption occurred very slowly. It can be correlated to the small pore volume of SX6 compared to others, inhibiting the molecule diffusion to the internal surface and reducing the mass transfer of water. At RH = 70% and 80%, the adsorption capacity trend of SX is similar. SX8 exhibits the highest humidity adsorption in the difference of relative humidity (RH). The large surface area of SX8 provides more active sites to capture the water molecule via hydrogen bridge formation [50]. Besides, a large pore volume also promotes the diffusion process of water molecules to the internal surface of SX8 [38], consequently enhancing the water adsorption on the SX8 surface. This result also reveals that pH 8 is the optimum condition to prepare SX. Interestingly, the adsorption capacity of SX10 is higher than that of SX7 at RH = 80% and 90%, indicating that the base nature of SX10 promotes water adsorption. However, the adsorption ability of SX6 is low at RH = 80% and 90% compared to others. The presence of proton in pH solution of SX6 inhibits the water adsorption via hydrogen bridge generation. As a result, the adsorption capacity of SX6 was reduced even though SX6 has a high surface area compared to SX7, SX9, and SX10. It can be summarized that the affecting factor for humidity adsorption is not only the surface area of the sample but also the nature properties of sample surface. The presence of proton on surface of sample is led to the repulsion force between $H^+$ and $[H_3O]^+$, and as a result, the adsorption is inhibited. Therefore, the synergistic between surface area and nature surface properties is very beneficial to enhance the humidity adsorption, which is shown by SX8. Based on the explanation, the illustration of the adsorption mechanism is depicted in Fig. 6. Humidity adsorption occurs due to the interaction between water molecules and silica surfaces

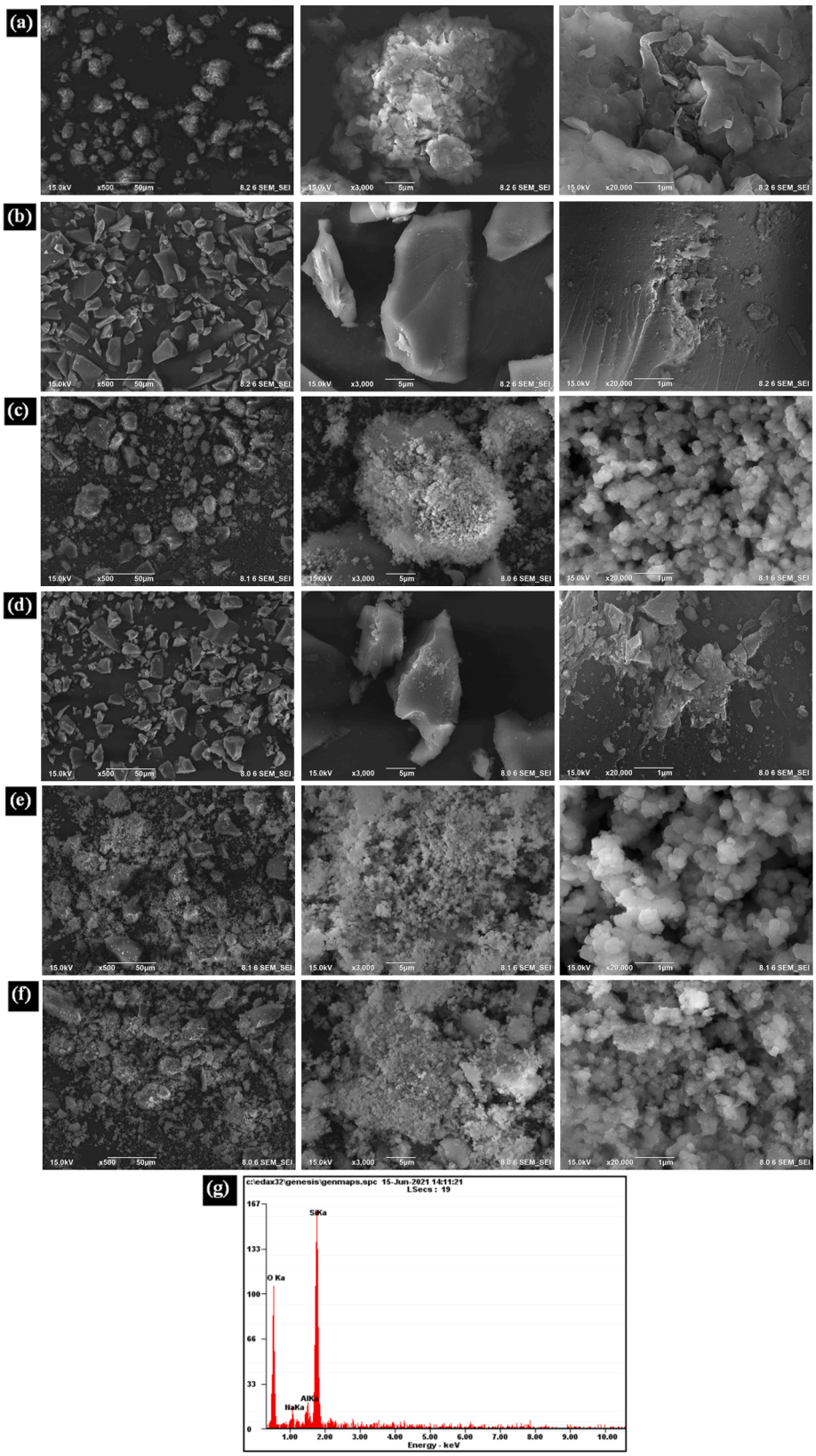


**Fig. 4.** FESEM micrograph of (a) VM, (b) SX6, (c) SX7, (d) SX8, (e) SX9, dan (f) SX10. (g) EDX spectra of SX8. Left: survey image of micromorphology. Middle and right: details of the particle's surfaces.

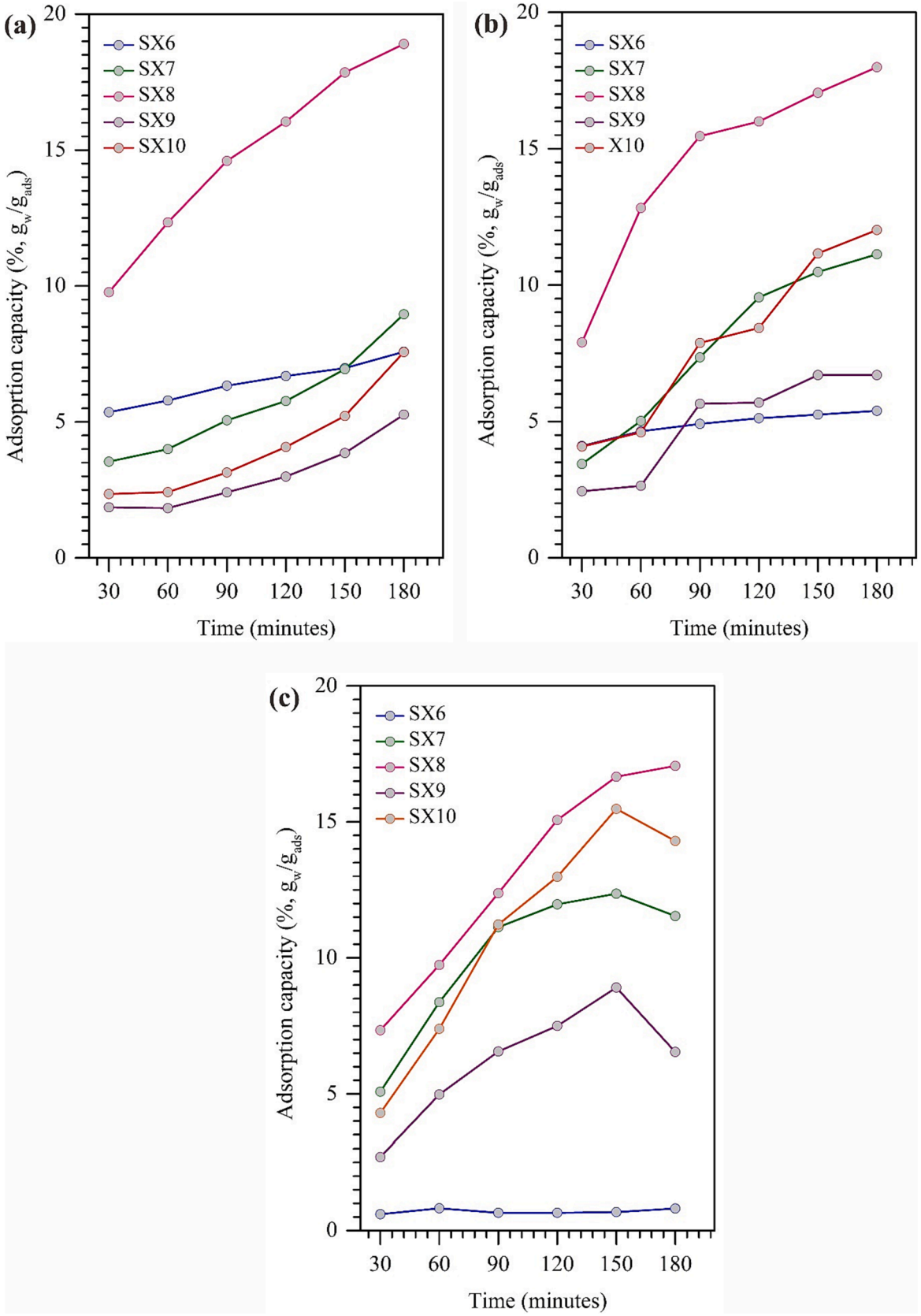


**Fig. 5.** Humidity adsorption of SX at RH of (a) 70%, (b) 80%, and (c) 90%.

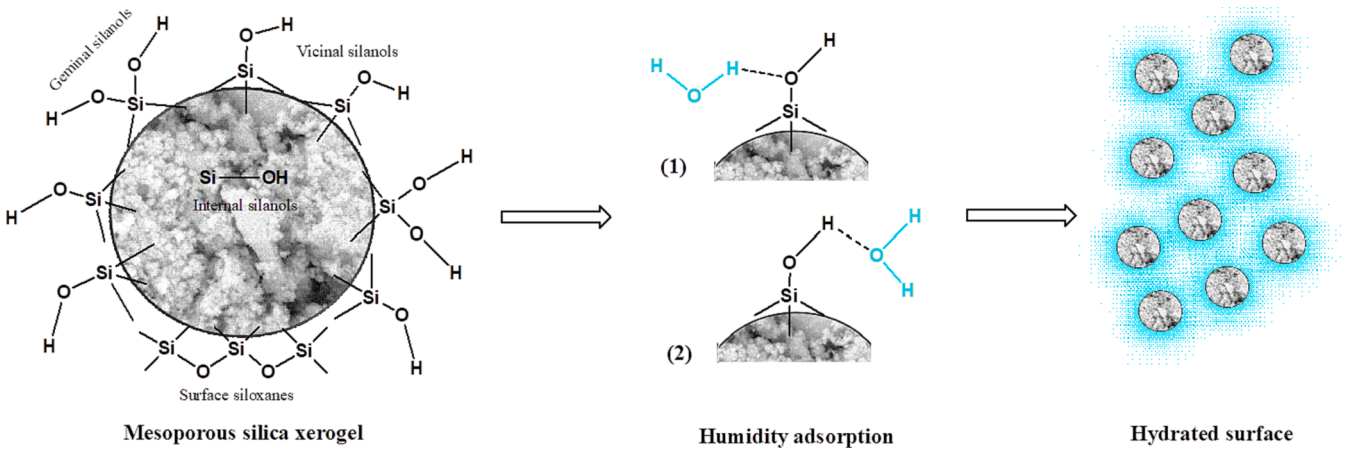


**Fig. 6.** Proposed mechanism of humidity adsorption using SX.

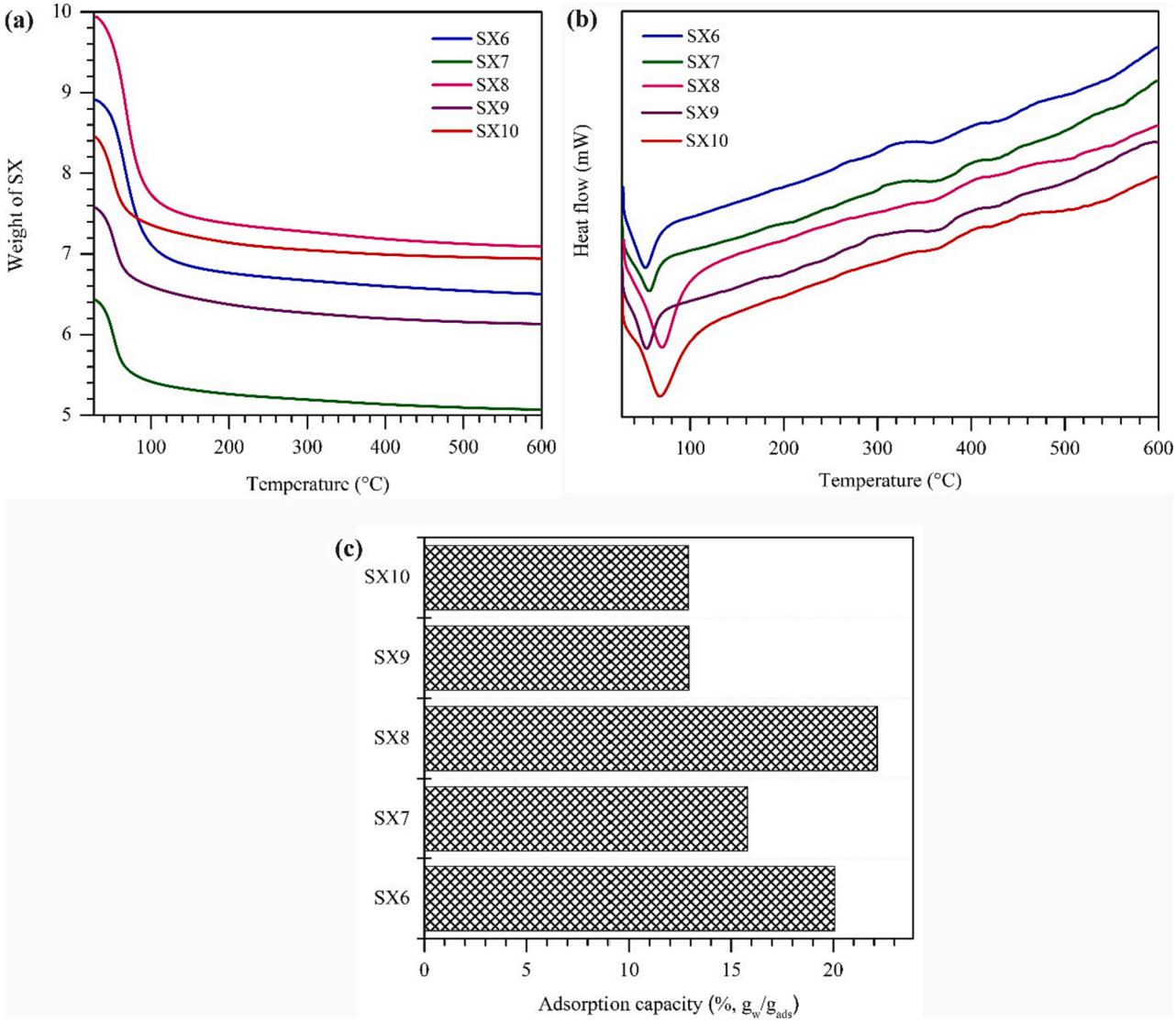


**Fig. 7.** (a) TGA profile of SX, (b) DTA profile of SX, and (c) its adsorption capacity calculated by the weight loss at 100 °C.

containing silanol and/or siloxane groups through lone pair electrons of oxygen in the silanol or siloxane groups with the hydrogen in water (Fig. 6a) and the hydrogen in silanol groups with the oxygen in water molecules (Fig. 6b). This process leads to the hydration of SX surface.

### 3.2.2. TG analysis

TG analysis was carried out to determine the amount of water desorbed from silica xerogel, as depicted in Fig. 7. All samples showed a type II TGA curve, suggesting the desorption of water or drying process

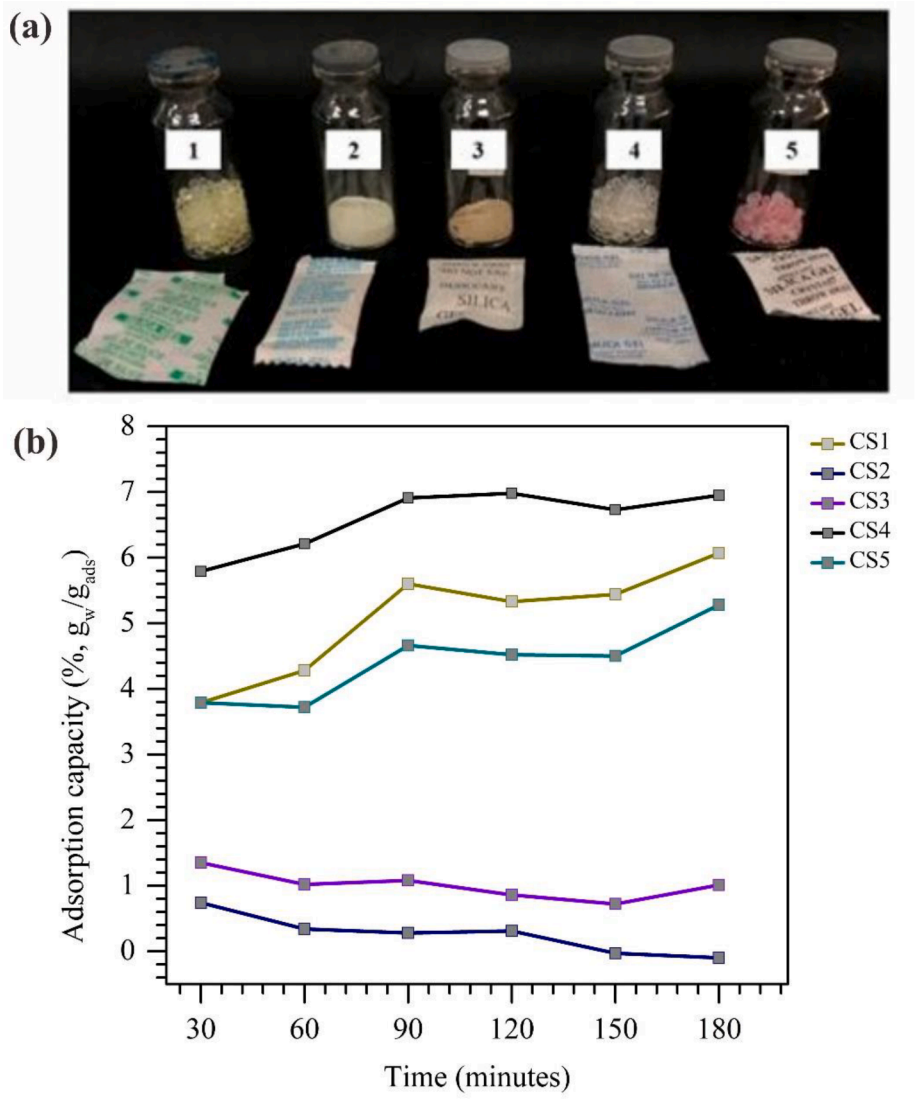


**Fig. 8.** (a) Various commercial silica (CS) and (b) their adsorption performance.

occurred. Those processes can be observed by weight loss at a temperature range of 30–120 °C, associated with the desorption of physically adsorbed water. All samples also exhibited a weight loss at temperature range of 130–400 °C, indicating the desorption of chemically adsorbed water on SX. These data are supported by the DTA results in Fig. 7b, which shows the presence of an initial downward curve indicating a thermal desorption process by the sample at 100 °C as an endothermic dehydration event [51]. The capacity of humidity adsorption was calculated from the weight loss at 100 °C. As shown in Fig. 7c, SX8 shows the highest water adsorption with 22.14% water capacity, followed by SX6 (20.07%), SX7 (15.79%), SX9 (12.92%), and SX10 (12.90%). The data obtained from TG analysis were in agreement with the conventional methods, in which SX8 exhibits the highest water adsorption capacity. The trend of TG analysis results of SX6 to SX10 agrees with the trend of their specific surface area as shown in Fig. 3. SX9 and SX10 exhibit similar efficiency due to the similar pore volume of SX9 and SX10.

The commercial silica gels were also investigated on their ability towards humidity adsorption to compare their ability with the prepared silica xerogel (SX8 as the optimum silica xerogel). Five types of commercial silica gel was tested at the optimum RH as depicted in Fig. 8. All commercial silica gel exhibited a lower adsorption capacity at 0.9–7% $g_{water}/g_{adsorbent}$ than the SX8, indicating the synthesized silica xerogel has more advantageous characteristics for humidity adsorption, such as active site or textural properties, so this result suggests SX8 potential applicable for commercialization.

## 4. Conclusion

A facile method for transforming volcanic mud into mesoporous silica xerogel has been carried out using sol–gel methods. The variation of pH during the sol–gel synthesis modified the textural properties of silica. The incomplete crystallization process causes a decrease in surface area. Silica produced at pH 8 generates the highest specific surface area and mesopore surface area, promoting a high adsorption capacity at 18.19% $g_w/g_{ads}$ determined from the conventional method, and 22.14% $g_w/g_{ads}$ when analysed using the TGA method. The humidity adsorption capacity was also higher than that of commercial silica gels, suggesting the potential of SX8 for commercialization. Additionally, the utilization of VM as a precursor would be beneficial to reduce the cost of production. However, it might be challenging to obtain high purity of SX because the presence of Al element in VM is difficult to remove.

## CRediT authorship contribution statement

**Qurrota A'yuni:** Conceptualization, Methodology, Investigation,

Validation, Funding acquisition, Writing - original draft. **Ardhana Rahmayanti:** Formal analysis, Investigation. **Hartati Hartati:** Supervision, Writing – review & editing. **Purkan Purkan:** Validation, Supervision. **Riki Subagyo:** Data curation, Writing – original draft. **Sofia Fuadah:** Investigation, Writing – original draft. **Novia Amalia Sholeha:** Formal analysis. **Hasliza Bahruji:** Writing – review & editing. **Hikmat Hikmat:** Formal analysis.

## Declaration of Competing Interest

The authors declare that they have no known competing financial interests or personal relationships that could have appeared to influence the work reported in this paper.

## Acknowledgements

The authors would like to acknowledge financial support from the Ministry of Education, Culture, Research, and Technology, Republic of Indonesia through the Penelitian Kerjasama Antar Perguruan Tinggi (PKPT) with contract number 001/U9.6/KP-PKPT/2020.

## References

[1] S. Zheng, J. Zhang, J. Mou, W. Du, Y. Yu, L. Wang, The influence of relative humidity and ground material on indoor walking-induced particle resuspension, J. Environ. Sci. Heal. - Part A Toxic/Hazardous Subst, Environ. Eng. 54 (2019) 1044–1053, https://doi.org/10.1080/10934529.2019.1644120.

[2] J. Chen, Q. Yu, M. Li, S. Sun, D. Zhan, Y. Wang, Z. Gu, Y. Zhang, Preparation of high specific surface area activated carbon fiber by high-temperature vacuum activation and its superior water vapor adsorption for air humidity control, J. Mater. Sci. 58 (2023) 2469–2493, https://doi.org/10.1007/s10853-023-08205-z.

[3] M. Faegh, P. Behnam, M.B. Shafii, A review on recent advances in humidification-dehumidification (HDH) desalination systems integrated with refrigeration, power and desalination technologies, Energy Convers. Manag. 196 (2019) 1002–1036, https://doi.org/10.1016/j.enconman.2019.06.063.

[4] M. Amani, S. Foroushani, M. Sultan, M. Bahrami, Comprehensive review on dehumidification strategies for agricultural greenhouse applications, Appl. Therm. Eng. 181 (2020), 115979, https://doi.org/10.1016/j.applthermaleng.2020.115979.

[5] B. Su, W. Han, H. Jin, An innovative solar-powered absorption refrigeration system combined with liquid desiccant dehumidification for cooling and water, Energy Convers. Manag. 153 (2017) 515–525, https://doi.org/10.1016/j.enconman.2017.10.028.

[6] W. Su, X. Zhang, Thermodynamic analysis of a compression-absorption refrigeration air-conditioning system coupled with liquid desiccant dehumidification, Appl. Therm. Eng. 115 (2017) 575–585, https://doi.org/10.1016/j.applthermaleng.2016.12.071.

[7] X.N. Wu, T.S. Ge, Y.J. Dai, R.Z. Wang, Review on substrate of solid desiccant dehumidification system, Renew. Sustain. Energy Rev. 82 (2018) 3236–3249, https://doi.org/10.1016/j.rser.2017.10.021.

[8] K.S. Rambhad, P.V. Walke, D.J. Tidke, Solid desiccant dehumidification and regeneration methods - A review, Renew. Sustain. Energy Rev. 59 (2016) 73–83, https://doi.org/10.1016/j.rser.2015.12.264.

[9] M.M. Abd-Elhady, M.S. Salem, A.M. Hamed, I.I. El-Sharkawy, Solid desiccant-based dehumidification systems: A critical review on configurations, techniques, and current trends, Int. J. Refrig. 133 (2022) 337–352, https://doi.org/10.1016/j.ijrefrig.2021.09.028.

[10] Z. Liu, C. Cheng, J. Han, X. Qi, Z. Zhao, R. Teng, Dehumidification performance of aluminum fumarate metal organic framework and its composite, Appl. Therm. Eng. 199 (2021), 117570, https://doi.org/10.1016/j.applthermaleng.2021.117570.

[11] L. Liu, S. (Johnathan) Tan, T. Horikawa, D.D. Do, D. Nicholson, J. Liu, Water adsorption on carbon - A review, Adv. Colloid Interface Sci. 250 (2017) 64–78. https://doi.org/10.1016/j.cis.2017.10.002.

[12] X. Zheng, T.S. Ge, R.Z. Wang, Recent progress on desiccant materials for solid desiccant cooling systems, Energy. 74 (2014) 280–294, https://doi.org/10.1016/j.energy.2014.07.027.

[13] B. Sun, A. Chakraborty, Thermodynamic frameworks of adsorption kinetics modeling: Dynamic water uptakes on silica gel for adsorption cooling applications, Energy. 84 (2015) 296–302, https://doi.org/10.1016/j.energy.2015.02.101.

[14] I.A. Simonova, A. Freni, G. Restuccia, Y.I. Aristov, Water sorption on composite "silica modified by calcium nitrate", Microporous Mesoporous Mater. 122 (2009) 223–228, https://doi.org/10.1016/j.micromeso.2009.02.034.

[15] L.W. Wang, R.Z. Wang, R.G. Oliveira, A review on adsorption working pairs for refrigeration, Renew. Sustain. Energy Rev. 13 (2009) 518–534, https://doi.org/10.1016/j.rser.2007.12.002.

[16] S. Rovani, J.J. Santos, P. Corio, D.A. Fungaro, Highly Pure Silica Nanoparticles with High Adsorption Capacity Obtained from Sugarcane Waste Ash, ACS Omega. 3 (2018) 2618–2627, https://doi.org/10.1021/acsomega.8b00092.

[17] S. Islam, Impact of pH on structural and sensing characteristics of cresol red encapsulated polyethylene glycol assisted silica nanomatrix: Sol-gel method, Opt. Mater. (Amst). 121 (2021), 111546, https://doi.org/10.1016/j.optmat.2021.111546.

[18] F.F. De Oliveira, K.O. Moura, L.S. Costa, C.B. Vidal, A.R. Loiola, R.F. Do Nascimento, Reactive Adsorption of Parabens on Synthesized Micro- And Mesoporous Silica from Coal Fly Ash: PH Effect on the Modification Process, ACS Omega. 5 (2020) 3346–3357. https://doi.org/10.1021/acsomega.9b03537.

[19] G. Guzel Kaya, H. Deveci, Synergistic effects of silica aerogels/xerogels on properties of polymer composites: A review, J. Ind. Eng. Chem. 89 (2020) 13–27, https://doi.org/10.1016/j.jiec.2020.05.019.

[20] S.S. Owoeye, F.I. Jegede, S.G. Borisade, Preparation and characterization of nano-sized silica xerogel particles using sodium silicate solution extracted from waste container glasses, Mater. Chem. Phys. 248 (2020), 122915, https://doi.org/10.1016/j.matchemphys.2020.122915.

[21] G. Guzel Kaya, E. Yilmaz, H. Deveci, Synthesis of sustainable silica xerogels/aerogels using inexpensive steel slag and bean pod ash: A comparison study, Adv. Powder Technol. 31 (2020) 926–936, https://doi.org/10.1016/j.apt.2019.12.013.

[22] D. Cyranoski, Muddy waters, Nature. 445 (2007) 812–815, https://doi.org/10.1038/445812a.

[23] A.A. Jalil, S. Triwahyono, S.H. Adam, N.D. Rahim, M.A.A. Aziz, N.H.H. Hairom, N. A.M. Razali, M.A.Z. Abidin, M.K.A. Mohamadiah, Adsorption of methyl orange from aqueous solution onto calcined Lapindo volcanic mud, J. Hazard. Mater. 181 (2010) 755–762, https://doi.org/10.1016/j.jhazmat.2010.05.078.

[24] S. Muljani, H. Setyawan, G. Wibawa, A. Altway, A facile method for the production of high-surface-area mesoporous silica gels from geothermal sludge, Adv. Powder Technol. 25 (2014) 1593–1599, https://doi.org/10.1016/j.apt.2014.05.012.

[25] P.E. Imoisili, K.O. Ukoba, T.C. Jen, Green technology extraction and characterisation of silica nanoparticles from palm kernel shell ash via sol-gel, J. Mater. Res. Technol. 9 (2020) 307–313, https://doi.org/10.1016/j.jmrt.2019.10.059.

[26] M.V. Khedkar, S.A. Jadhav, S.B. Somvanshi, P.B. Kharat, K.M. Jadhav, Physicochemical properties of ambient pressure dried surface modified silica aerogels: effect of pH variation, SN Appl. Sci. 2 (2020) 1–10, https://doi.org/10.1007/s42452-020-2463-3.

[27] J.A. Bush, J. Vanneste, E.M. Gustafson, C.A. Waechter, D. Jassby, C.S. Turchi, T. Y. Cath, Prevention and management of silica scaling in membrane distillation using pH adjustment, J. Memb. Sci. 554 (2018) 366–377, https://doi.org/10.1016/j.memsci.2018.02.059.

[28] S. Affandi, H. Setyawan, S. Winardi, A. Purwanto, R. Balgis, A facile method for production of high-purity silica xerogels from bagasse ash, Adv. Powder Technol. 20 (2009) 468–472, https://doi.org/10.1016/j.apt.2009.03.008.

[29] N.B. Talib, S. Triwahyono, A.A. Jalil, C.R. Mamat, N. Salamun, N.A.A. Fatah, S. M. Sidik, L.P. Teh, Utilization of a cost effective Lapindo mud catalyst derived from eruption waste for transesterification of waste oils, Energy Convers. Manag. 108 (2016) 411–421, https://doi.org/10.1016/j.enconman.2015.11.031.

[30] A. Rahmayanti, Q. A'yuni, H. Hartati, P. Purkan, I.G. Romanza, Synthesis and characterization of silica gel from Lapindo mud Sidoarjo, IOP Conf. Ser. Earth Environ. Sci. 456 (1) (2020), 012007, https://doi.org/10.1088/1755-1315/456/1/012007.

[31] U. Zulfiqar, T. Subhani, S.W. Husain, Synthesis and characterization of silica nanoparticles from clay, J. Asian Ceram. Soc. 4 (2016) 91–96, https://doi.org/10.1016/j.jascer.2015.12.001.

[32] U. Zulfiqar, T. Subhani, S. Wilayat Husain, Synthesis of silica nanoparticles from sodium silicate under alkaline conditions, J. Sol-Gel Sci. Technol. 77 (2016) 753–758, https://doi.org/10.1007/s10971-015-3950-7.

[33] U. Zulfiqar, T. Subhani, S. Wilayat Husain, Towards tunable size of silica particles from rice husk, J. Non. Cryst. Solids. 429 (2015) 61–69, https://doi.org/10.1016/j.jnoncrysol.2015.08.037.

[34] S. Steven, E. Restiawaty, P. Pasymi, Y. Bindar, An appropriate acid leaching sequence in rice husk ash extraction to enhance the produced green silica quality for sustainable industrial silica gel purpose, J. Taiwan Inst. Chem. Eng. 122 (2021) 51–57, https://doi.org/10.1016/j.jtice.2021.04.053.

[35] H.U. Hambali, A.A. Jalil, S. Triwahyono, S.F. Jamian, N.A.A. Fatah, A. A. Abdulrasheed, T.J. Siang, Unique structure of fibrous ZSM-5 catalyst expedited prolonged hydrogen atom restoration for selective production of propylene from methanol, Int. J. Hydrogen Energy. 46 (2021) 24652–24665, https://doi.org/10.1016/j.ijhydene.2019.11.236.

[36] I.F. Ulfindrayani, A. Zulys, F. Kurniawan, Q. A'yuni, H. Pardi, I.K. Murwani, Lanthanum phosphate as catalyst in the reaction of 5-HMF formation, BIO Web Conf. 70 (2023), 03009, https://doi.org/10.1051/bioconf/20237003009.

[37] H. Tehubijuluw, R. Subagyo, Y. Kusumawati, D. Prasetyoko, The impregnation of ZnO onto ZSM-5 derived from red mud for photocatalytic degradation of methylene blue, Sustain. Environ. Res. 32 (2022), https://doi.org/10.1186/s42834-021-00113-8.

[38] H. Tehubijuluw, R. Subagyo, M.F. Yulita, R.E. Nugraha, Y. Kusumawati, H. Bahruji, A.A. Jalil, H. Hartati, D. Prasetyoko, Utilization of red mud waste into mesoporous ZSM-5 for methylene blue adsorption-desorption studies, Environ. Sci. Pollut. Res. 28 (2021) 37354–37370, https://doi.org/10.1007/s11356-021-13285-y.

[39] R. Subagyo, H. Tehubijuluw, W. Prasetyo Utomo, H. Dwi Rizqi, Y. Kusumawati, H. Bahruji, D. Prasetyoko, Converting red mud wastes into mesoporous ZSM-5 decorated with TiO2 as an eco-friendly and efficient adsorbent-photocatalyst for dyes removal, Arab. J. Chem. 15 (2022), 103754, https://doi.org/10.1016/j.arabjc.2022.103754.

[40] S. Suttiruengwong, S. Pivsa-Art, M. Chareonpanich, Hydrophilic and hydrophobic mesoporous silica derived from rice husk ash as a potential drug carrier, Materials (Basel). 11 (2018), https://doi.org/10.3390/ma11071142.
[41] D. Prasetyoko, N.A. Sholeha, R. Subagyo, M. Ulfa, H. Bahruji, H. Holilah, M. F. Pradipta, A.A. Jalil, Mesoporous ZnO nanoparticles using gelatin — Pluronic F127 as a double colloidal system for methylene blue photodegradation, Korean J. Chem. Eng. 40 (2023) 112–123, https://doi.org/10.1007/s11814-022-1224-y.
[42] H. Hartati, Q. A'yuni, N.H. Saputri, D.Z. Mardho, P.B.D. Firda, H. Hartono, H. Bahruji, R.E. Nugraha, N.A. Sholeha, D. Prasetyoko, Aluminosilicates Catalysts Synthesis from Low-Grade Indonesian Kaolin for the Acetalization Reaction, Catalysts. 13 (2023) 122, https://doi.org/10.3390/catal13010122.
[43] R.K. Iler, The Chemistry of Silica: Solubility, Polymerization, Colloid and Surface Properties and Biochemistry of Silica, John Wiley & Sons, Inc., New York, 1979.
[44] Y.P. Lestari, A. Amaria, Effect of Ammonia-Ethanol Mole Ratio on the Silica Nanoparticles Synthesized for Rhodamine B Dyes Adsorption, J. Kim. Ris. 8 (2023) 92–104, https://doi.org/10.20473/jkr.v8i1.44400.
[45] P. Albers, M. Maier, M. Reisinger, B. Hannebauer, R. Weinand, Physical boundaries within aggregates - Differences between amorphous, para-crystalline, and crystalline Structures, Cryst. Res. Technol. 50 (2015) 846–865, https://doi.org/10.1002/crat.201500040.
[46] C.O. Prempeh, I. Hartmann, S. Formann, M. Eiden, K. Neubauer, H. Atia, A. Wotzka, S. Wohlrab, M. Nelles, Comparative Study of Commercial Silica and Sol-Gel-Derived Porous Silica from Cornhusk for Low-Temperature Catalytic Methane Combustion, Nanomaterials. 13 (2023), https://doi.org/10.3390/nano13091450.
[47] G. Sriram, U.T. Uthappa, M. Kigga, H.Y. Jung, T. Altalhi, V. Brahmkhatri, M. D. Kurkuri, Xerogel activated diatoms as an effective hybrid adsorbent for the efficient removal of malachite green, New J. Chem. 43 (2019) 3810–3820, https://doi.org/10.1039/c9nj00015a.
[48] G. Sriram, M.P. Bhat, M. Kigga, U.T. Uthappa, H.Y. Jung, T. Kumeria, M. D. Kurkuri, Amine activated diatom xerogel hybrid material for efficient removal of hazardous dye, Mater. Chem. Phys. 235 (2019), 121738, https://doi.org/10.1016/j.matchemphys.2019.121738.
[49] R.K. Johnston, J.C. Harper, M.S. Tartis, Control over Silica Particle Growth and Particle-Biomolecule Interactions Facilitates Silica Encapsulation of Mammalian Cells with Thickness Control, ACS Biomater. Sci. Eng. 3 (2017) 2098–2109, https://doi.org/10.1021/acsbiomaterials.7b00185.
[50] P. Kumar, S. Kumar, A. Kumar, V. Verma, Lithium-doped SnO2 porous ceramics-based hydroelectric cells: a novel green energy source for sustainable power generation, J. Mater. Sci. Mater. Electron. 32 (2021) 14833–14845, https://doi.org/10.1007/s10854-021-06037-8.
[51] Q. A'yuni, A. Rahmayanti, H. Hartati, P. Purkan, R. Subagyo, N. Rohmah, L. R. Itsnaini, M.A. Fitri, Synthesis and characterization of silica gel from Lapindo volcanic mud with ethanol as a cosolvent for desiccant applications, RSC Adv. 13 (2023) 2692–2699, https://doi.org/10.1039/d2ra07891k.